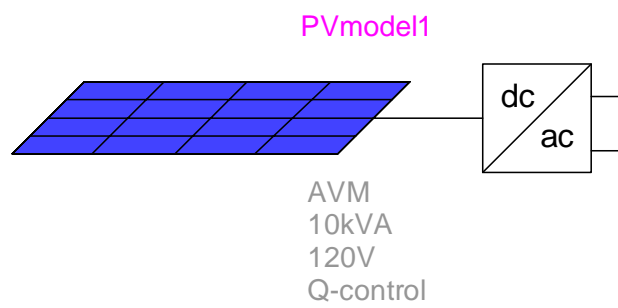


PV Single-phase Model in EMTP®



Henry Gras, Ilhan Kocar, Ulas Karaagac, Jean Mahseredjian

1	INTRODUCTION	4
1.1	GENERAL	4
1.2	PV MODULE.....	4
1.2.1	Parameters	4
1.2.2	Diode parameters	5
1.2.3	Definition of <i>R_p</i>	6
1.2.4	Definition of <i>I_{ph}</i>	6
1.2.5	Final Solution	6
2	ELECTRICAL CIRCUIT.....	9
2.1	REACTIVE POWER CONTROL IN SOLAR PANELS	10
2.2	PV INVERTER CONTROL AND PROTECTION SYSTEMS.....	11
3	EMTP® IMPLEMENTATION	14
3.1	DETAILED AND AVERAGE VALUE MODELS.....	14
3.2	SOLAR PANEL MODEL IN EMTP®.....	16
3.2.1	Solar panel Control System Block.....	16
3.2.2	PV Electrical System.....	17
3.2.3	PV inverter Control System Block	19
3.2.3.1	PV inverter Grid Side Converter Control	20
3.2.4	PV inverter Protection System Block.....	23
3.2.4.1	Overvoltage and Undervoltage protections	24
3.2.4.2	dc Overvoltage Protection Block.....	26
3.2.4.3	Overcurrent Protection Block.....	27
4	REFERENCES	28

Table of Figures

Figure 1	Equivalent circuit of a PV array	4
Figure 2	Behaviour of $f(R_s)$ on studied interval.....	7
Figure 3	Equivalent electrical circuit of a PV array	9
Figure 4	Current source subcircuit.....	9
Figure 5	Diode subcircuit.....	10
Figure 6	Reactive power control function	11
Figure 7	Solar panel configuration	11
Figure 8	Simplified diagram of inverter control and protection system	12
Figure 9	Schematic diagram of inverter control.....	13
Figure 10	Solar panel device.	14
Figure 11	dc-ac converter system block in PV models (detailed model version)	15
Figure 12	(a) Two-level Converter, (b) IGBT valve.....	15
Figure 13	PWM control block.....	15
Figure 14	dc-ac converter system block in PV models (average value model version)	15
Figure 15	EMTP® diagram of the Solar panel.....	16
Figure 16	EMTP® diagram of the Q-control block.....	17
Figure 17	EMTP® diagram of the Solar panel.....	18
Figure 18	“shunt ac harmonic filter” block	19
Figure 19	EMTP® diagram of the PV inverter control block.....	19
Figure 20	EMTP diagram of the PLL.....	20
Figure 21	EMTP® diagram of PV inverter “Grid Control” block.....	20
Figure 22	GSC arrangement	21
Figure 23	PV inverter reactive output current during voltage disturbances [16].....	22
Figure 24	EMTP® diagram of “ I_{dq} reference limiter” block.....	22
Figure 25	EMTP® diagram of “FRT decision logic” block.....	23
Figure 26	EMTP® diagram of protection system block.....	23
Figure 27	Protection system parameters	24
Figure 28	EMTP® diagram of overvoltage and undervoltage protections	25
Figure 29	Transient overvoltage limits	25
Figure 30	LVRT and HVRT requirements [19]	26
Figure 31	EMTP® diagram of dc overvoltage protection block	26
Figure 32	EMTP® diagram of overcurrent protection block	27

1 INTRODUCTION

The single-phase PV is a model of a few kW household single-phase inverter. The model is built for 120/240V split phase and possesses 2 connection ports: L1(+120VRMS) and L2(-120VRMS). It is possible to plug it to a 208VRMSLL network by connecting L1 to a phase and L2 to another.

1.1 General

1.2 PV module

1.2.1 Parameters

This report presents the modeling of PV arrays in EMTP® just by using the manufacturer's datasheet. The model is an equivalent electrical circuit with one nonlinear diode as illustrated in Figure 1:

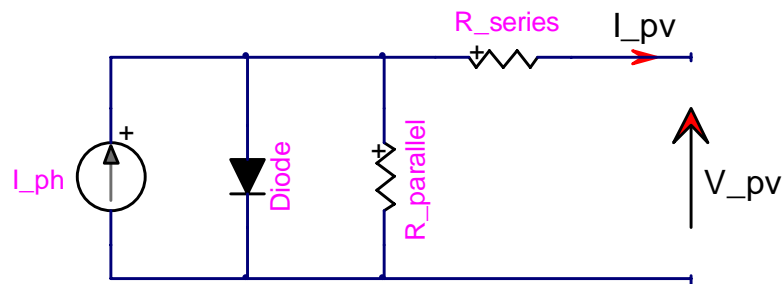


Figure 1 Equivalent circuit of a PV array

The electrical parameters of the components in the equivalent circuit are not readily available in datasheets. This report explains how to obtain the parameters using the datasheet information only and without performing any physical experiments.

First, the available information in datasheets, useful for the computation of parameters, is defined:

P_{max} : **Maximum power**

V_{maxP} : **Voltage at maximum power**

I_{maxP} : **Current at maximum power**

V_{oc} : **Open circuit voltage**

I_{sc} : **Short circuit current**

K_i : **Temperature coefficient of short circuit current**

K_v : **Temperature coefficient of open circuit voltage**

N_s : **Number of cells per module** (in series)

All these data are given for standard test conditions, obtained at a temperature of 25°C and for an irradiance of 1000 W/m².

$$T_{ref} = 25^{\circ}C \quad G_{ref} = 1000W / m^2$$

One last data which is defined indirectly by the datasheet is the **ideal factor** a . This factor depends on the PV cell technology. A table in [1] gives the value of ideal factor for different PV technologies. This factor also varies with the irradiance [2], but the variation is low and it is considered constant in our model.

Finally, the actual atmospheric conditions are required: **temperature** T and **irradiance** G . Temperature is considered constant during time domain simulations given the time frame of typical EMT-type studies.

The **irradiance**, however, can be constant or variable as defined by the user. More details are given at the end this document.

The relation between I_{PV} and V_{PV} in Figure 1 is given by:

$$I_{PV} = I_{ph} - I_{diode} - \frac{V_{PV} + I_{PV}R_s}{R_p} \quad (1)$$

where I_{diode} is the current flowing through the diode, R_s is the series resistance and R_p is the parallel resistance.

The next part explains how to obtain these electrical parameters.

1.2.2 Diode parameters

First, diode parameters need to be calculated using the standard conditions data (usually an irradiance of 1000 W/m² and a temperature of 25°C).

$$I_{diode} = I_0 \left[\exp\left(\frac{V_{diode}}{aN_sV_{th}}\right) - 1 \right] \quad (2)$$

where

$$V_{diode} = \frac{V_{PV} + I_{PV}R_s}{N_s} \quad (3)$$

The division by N_s is because we consider the diode for only one cell. As there are N_s cells in series, the voltage is equally divided on the N_s diodes.

The threshold voltage is:

$$V_{th} = \frac{kT_{ref}}{q} \quad (4)$$

where k is the Boltzmann's constant, q the charge of an electron and T_{ref} the reference temperature in Kelvin.

And the reversed saturation current is:

$$I_0 = \frac{I_{sc}}{\exp\left(\frac{V_{oc}}{aN_sV_{th}}\right) - 1} \quad (5)$$

From this, equation (1) becomes:

$$I_{PV} = I_{ph} - \frac{V_{PV} + I_{PV}R_s}{R_p} - I_0 \left[\exp\left(\frac{V_{PV} + I_{PV}R_s}{aN_sV_{th}}\right) - 1 \right] \quad (6)$$

In this equation there are still three unknown variables: I_{ph} , R_s and R_p .

To obtain these values the equations described in [3] are used. The equations are, however, solved here in a different way.

The goal here is to express I_{ph} and R_p in function of R_s . In such a case only one unknown variable remains, and the non-linear equation obtained can be solved with a numerical method.

Equation (6) is taken in maximum power conditions (voltage and current are given in datasheet) and from it a function f in function of R_s is defined:

$$f(R_s) = I_{ph} - I_{maxP} - \frac{V_{maxP} + I_{maxP}R_s}{R_p} - I_0 \left[\exp\left(\frac{V_{maxP} + I_{maxP}R_s}{aN_sV_{th}}\right) - 1 \right] \quad (7)$$

The objective here is to find such an R_s that the function f becomes zero.

1.2.3 Definition of R_p

To obtain this resistance another equation is required. The derivative of power with respect to voltage is used here. In maximal power condition, this derivative is zero.

$$0 = \frac{dP_{PV}}{dV_{PV}} \Big|_{max} = \frac{d(V_{PV}I_{PV})}{dV_{PV}} \Big|_{max} = I_{maxP} + V_{maxP} \left(\frac{dI_{PV}}{dV_{PV}} \right) \Big|_{max} \quad (8)$$

From (6) the derivative is calculated and taken in maximal power condition:

$$\left(\frac{dI_{PV}}{dV_{PV}} \right) \Big|_{max} = \frac{-aN_s V_{th} - R_p I_0 \exp\left(\frac{V_{maxP} + I_{maxP} R_s}{aN_s V_{th}}\right)}{R_p aN_s V_{th} + R_s aN_s V_{th} + R_p R_s I_0 \exp\left(\frac{V_{maxP} + I_{maxP} R_s}{aN_s V_{th}}\right)} \quad (9)$$

Equation (9) is inserted into (8) and R_p is isolated:

$$R_p = \frac{1}{\frac{I_{maxP}}{V_{maxP} - R_s I_{maxP}} - \frac{I_0}{aN_s V_{th}} \exp\left(\frac{V_{maxP} + I_{maxP} R_s}{aN_s V_{th}}\right)} \quad (10)$$

1.2.4 Definition of I_{ph}

As under short circuit conditions the voltage is low, the current flowing through the diode is negligible. In this case, there are only two resistances to be considered. As the short-circuit current is the one flowing in R_s we have:

$$I_{sc} = I_{ph} \frac{R_p}{R_s + R_p} \quad (11)$$

$$I_{ph} = I_{sc} \frac{R_s + R_p}{R_p} = I_{sc} \left(\frac{R_s}{R_p} + 1 \right) \quad (12)$$

By replacing R_p with (10):

$$I_{ph} = I_{sc} \left[1 + R_s \left(\frac{1}{\frac{V_{maxP}}{I_{maxP}} - R_s} - \frac{I_0}{aN_s V_{th}} \exp\left(\frac{V_{maxP} + I_{maxP} R_s}{aN_s V_{th}}\right) \right) \right] \quad (13)$$

After simplification:

$$I_{ph} = I_{sc} \left[\frac{V_{maxP}}{V_{maxP} - R_s I_{maxP}} - \frac{I_0 R_s}{aN_s V_{th}} \exp\left(\frac{V_{maxP} + I_{maxP} R_s}{aN_s V_{th}}\right) \right] \quad (14)$$

1.2.5 Final Solution

The parallel resistance and the current source are now defined as a function of the series resistance. Equations (10) and (14) are inserted into (7):

$$\begin{aligned}
f(R_s) = & -I_{maxP} + I_{sc} \left[\frac{V_{maxP}}{V_{maxP} - R_s I_{maxP}} - \frac{I_0 R_s}{aN_s V_{th}} \exp\left(\frac{V_{maxP} + I_{maxP} R_s}{aN_s V_{th}}\right) \right] \\
& - (V_{maxP} + I_{maxP} R_s) \left[\frac{I_{maxP}}{V_{maxP} - R_s I_{maxP}} - \frac{I_0}{aN_s V_{th}} \exp\left(\frac{V_{maxP} + I_{maxP} R_s}{aN_s V_{th}}\right) \right] \\
& - I_0 \left[\exp\left(\frac{V_{maxP} + I_{maxP} R_s}{aN_s V_{th}}\right) - 1 \right]
\end{aligned} \quad (15)$$

This expression is simplified to:

$$\begin{aligned}
f(R_s) = & \frac{V_{maxP}(I_{sc} + I_0 - 2I_{maxP}) - I_0 I_{maxP} R_s}{V_{maxP} - R_s I_{maxP}} \\
& + I_0 \exp\left(\frac{V_{maxP} + I_{maxP} R_s}{aN_s V_{th}}\right) \left[\frac{R_s(I_{maxP} - I_{sc}) + V_{maxP} - aN_s V_{th}}{aN_s V_{th}} \right]
\end{aligned} \quad (16)$$

The goal is to find the value of R_s such that f equals to zero. To solve this non-linear equation, Newton method is used. As this function crosses zero several times, a specific interval has to be chosen. Newton method can be used because f' and f'' are both strictly positive on the studied interval: $[0; R_{s-max}]$.

R_{s-max} is defined as:

$$R_{s-max} = \frac{V_{oc} - V_{maxP}}{I_{maxP}} - \frac{aN_s V_{th}}{I_0} \exp\left(\frac{-V_{oc}}{aN_s V_{th}}\right) \quad (17)$$

Here is an example of the behaviour of $f(R_s)$ on $[0; R_{s-max}]$ for a specific photovoltaic module (KC200GT Kyosera).

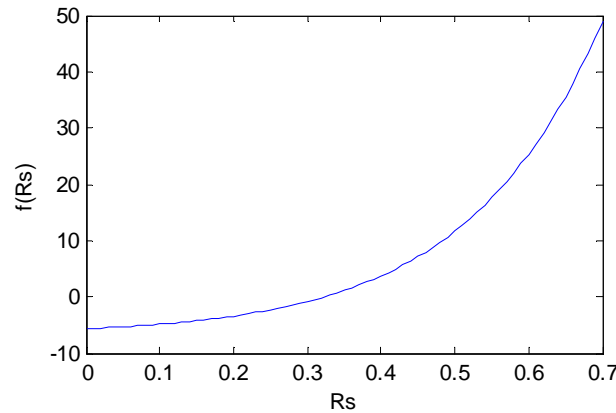


Figure 2 Behaviour of $f(R_s)$ on studied interval

To use Newton method the derivative of the function is required:

$$\begin{aligned}
\frac{df}{dR_s} = & \frac{I_{maxP} V_{maxP} (I_{sc} - 2I_{maxP})}{(V_{maxP} - R_s I_{maxP})^2} \\
& + I_0 \exp\left(\frac{V_{maxP} + I_{maxP} R_s}{aN_s V_{th}}\right) \left[\frac{-I_{sc} aN_s V_{th} + R_s I_{maxP} (I_{maxP} - I_{sc}) + I_{maxP} V_{maxP}}{(aN_s V_{th})^2} \right]
\end{aligned} \quad (18)$$

As f' is positive, initialization is done with the maximum value:

$$R_s^0 = R_{s-max} \quad (19)$$

The iterative procedure is:

$$R_s^{i+1} = R_s^i - \frac{f(R_s^i)}{f'(R_s^i)} \quad (20)$$

And it is stopped when the variation is below the tolerance ε :

$$R_s^i - R_s^{i+1} < \varepsilon \quad (21)$$

Once the iterative procedure yields the final value of R_s^i , it is possible to compute R_p and I_{ph} using equations (10) and (14).

As previous calculations were done under standard conditions, the current of the current source is abbreviated with I_{ph0} .

Parameters are now calculated for the actual atmospheric conditions:

$$V_{th} = \frac{kT}{q} \quad (22)$$

$$I_0 = \frac{I_{sc} + K_i(T - T_{ref})}{\exp\left(\frac{V_{oc} + K_v(T - T_{ref})}{aN_s V_{th}}\right) - 1} \quad (23)$$

$$I_{ph_T} = I_{ph0} + K_i(T - T_{ref}) \quad (24)$$

$$I_{ph} = I_{ph_T} \frac{G}{G_{ref}} \quad (25)$$

Here we have the parameters for the given conditions but for only one photovoltaic module. The total number of modules is calculated using the nominal DC voltage and the given output power of the plant.

$$N_{mod-s} = \frac{V_{DC}}{V_{maxP}} \quad N_{mod-p} = \frac{P_{plant}}{V_{DC} I_{maxP}} \quad (26)$$

where N_{mod-p} is the number of module in parallel and N_{mod-s} the number of module in series in the plant.

Parameters are updated for the last time:

$$I_{ph_tot} = I_{ph} N_{mod-p} \quad (27)$$

$$R_{s_tot} = \frac{N_{mod-s}}{N_{mod-p}} R_s \quad R_{p_tot} = \frac{N_{mod-s}}{N_{mod-p}} R_p \quad (28)$$

$$I_{0_tot} = N_{mod-p} I_0 \quad N_{s_tot} = N_s N_{mod-s} \quad (29)$$

$$I_{diodes} = I_{0_tot} \exp\left(\frac{V_{diodes}}{aN_{s_tot} V_{th}}\right) \quad (30)$$

Subscript "tot" is used to indicate that it is the final value that will be used in the model.

All electrical parameters are sent into the circuit.

2 Electrical circuit

The EMTP® circuit is presented in Figure 3.

As the diode is a non-linear device, it is moved inside the control block. So the current source showed in Figure 3 represents the photoelectric current source in parallel with the diode.

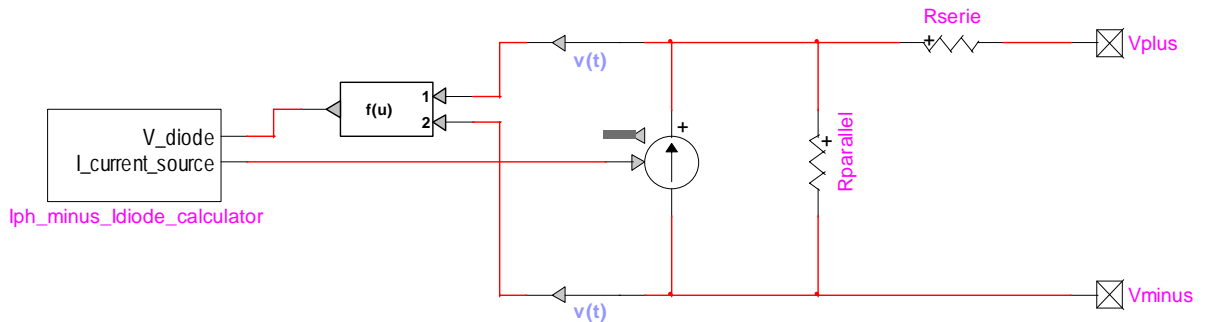


Figure 3 Equivalent electrical circuit of a PV array

The control block calculates the current from photoelectric cells and the current flowing through the diode. Then the diode current is subtracted from photoelectric current, and the resulting current drives the controlled current source in Figure 3.

Figure 4 presents the subcircuit which calculates photovoltaic current as a function of irradiance with respect to (25). Two modes are available: one with a constant irradiance and one with a variable irradiance. For variable mode, irradiance behaviour has to be entered in block “Ftb2” (on the down left corner). The temperature is considered constant during the simulation.

Figure 5 presents the subcircuit which calculates the diode current as a function of the diode voltage using (30).

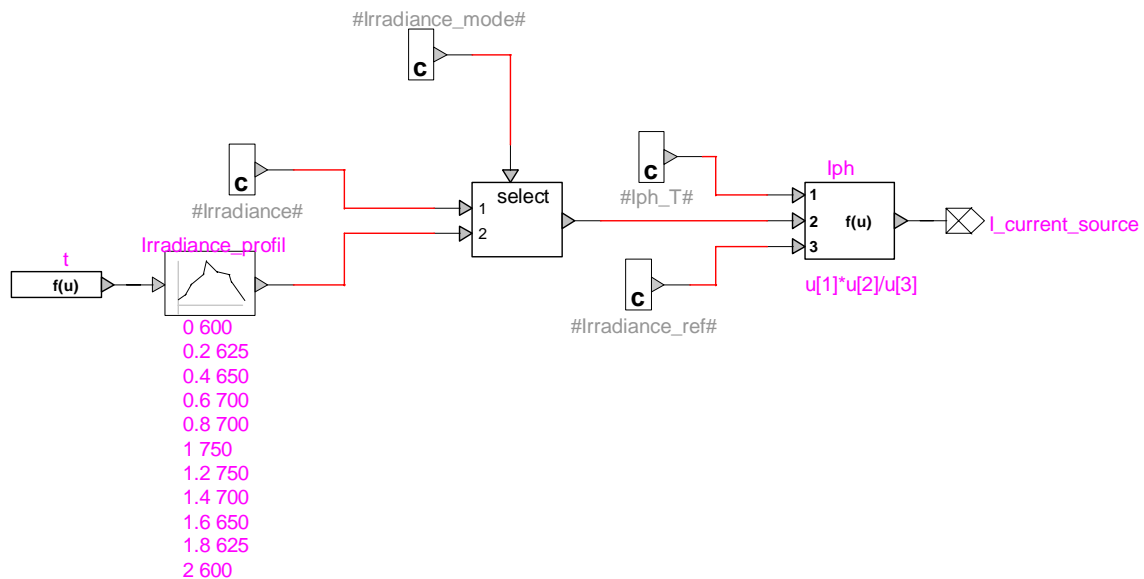


Figure 4 Current source subcircuit

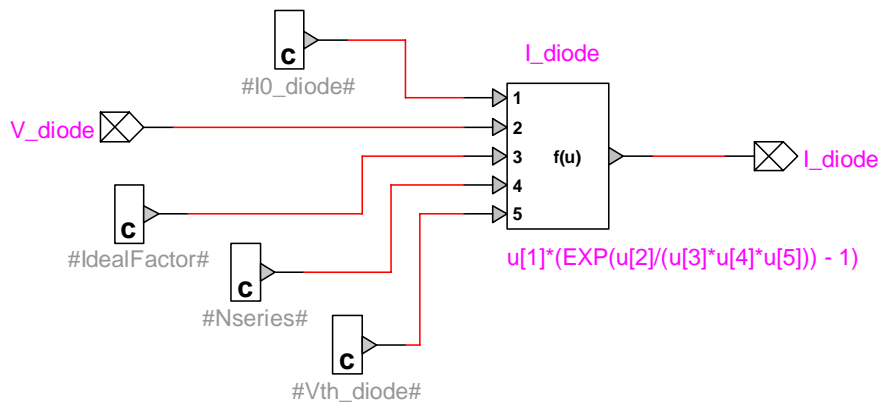


Figure 5 Diode subcircuit

2.1 Reactive Power Control in Solar panels

The active power at the point of interconnection depends on the weather conditions. However, according to customary grid code requirements, the Solar panel controls the reactive power at POI. 3 types of control are available:

- Q-control: where the reactive power reference is a user-defined parameter named **Initial reactive power**.
- V-control: where the reactive power reference is a function of the voltage. The function $Q=f(V)$ is defined in a table device named Q_function_of_V and can be modified by users.
- PF-control: where the power-factor is controlled.

The reactive power control function is located in Ctrl/Grid_Ctrl/GDC_outer_loop_Q. The scheme is presented in Figure 6.

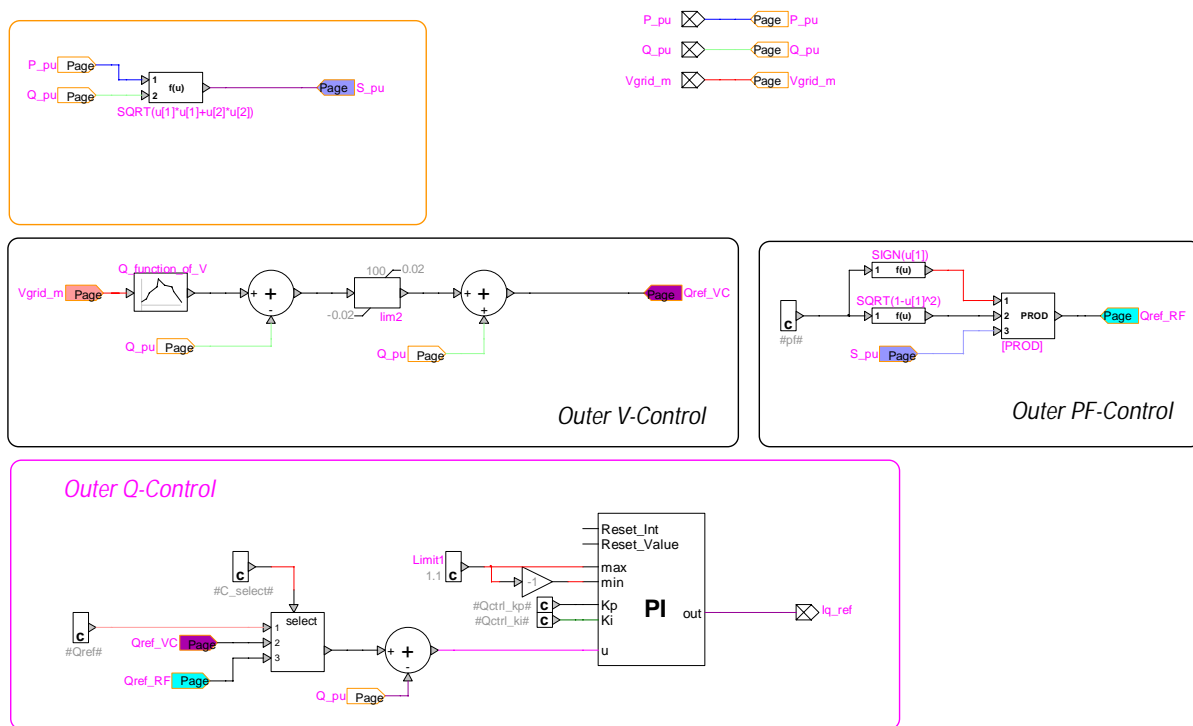


Figure 6 Reactive power control function

2.2 PV inverter control and protection systems

The considered topology is shown in Figure 7. It uses a dc-ac converter system consisting of a voltage source converter (VSC) on the grid side (GSC: Grid Side Converter). The dc resistive chopper is used for the dc bus overvoltage protection. A line inductor (choke filter) and an ac harmonic filter are used at the GSC to improve the power quality.

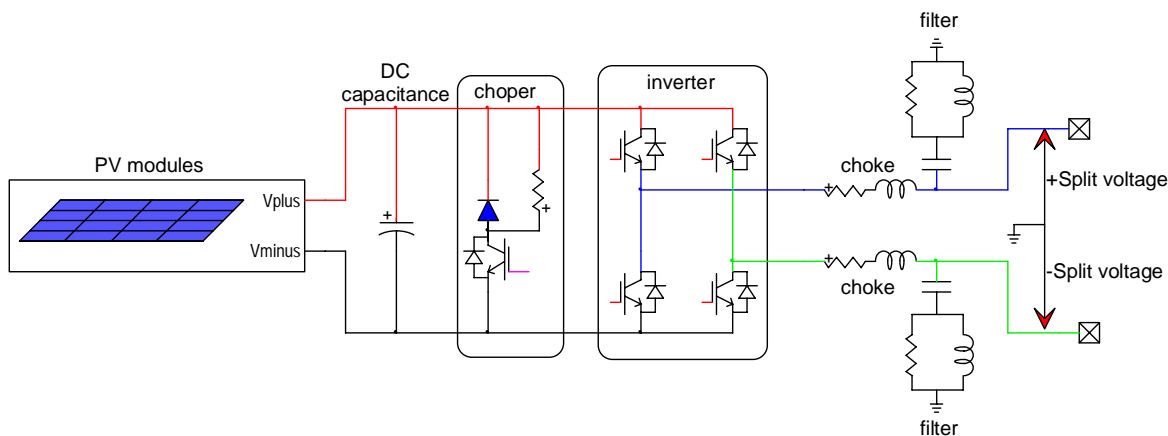


Figure 7 Solar panel configuration

The simplified diagram of PV inverter control and protection system is shown in Figure 8. The sampled signals are converted to per unit and filtered at “Measurements & Filters” block. The input measuring filters are low-pass (LP) type.

- “Compute Variables” block computes the variables used by the PV inverter control and protection system.

- “Protection System” block contains low voltage and overvoltage relays, GSC overcurrent protections and dc resistive chopper control.

The control of the PV inverter is achieved by controlling the GSC utilizing vector control techniques. Vector control allows decoupled control of real and reactive powers. The currents are projected on a rotating reference frame based on either ac flux or voltage. Those projections are referred to d- and q-components of their respective currents. In flux-based rotating frame, the q-component corresponds to real power and the d-component to reactive power. In voltage-based rotating frame (90° ahead of flux-based frame), the d and q components represent the opposite.

The control scheme is illustrated in Figure 9. In this figure, i_{qg} and i_{dg} are the q- and d-axis currents of the GSC, V_{dc} is the dc bus voltage, and V_{wt}^+ is the positive sequence voltage at Solar panel transformer MV terminal.

In the control scheme presented in Figure 9, the GSC operates in the stator voltage reference (SVR) frame. i_{dg} is used to maintain V_{dc} and i_{qg} is used to control V_{wt}^+ .

The GSC is controlled by a two-level controller. The slow outer control calculates the reference dq-frame currents (i'_{dg} and i'_{qg}) and the fast inner control allows controlling the converter ac voltage reference that will be used to generate the modulated switching pattern.

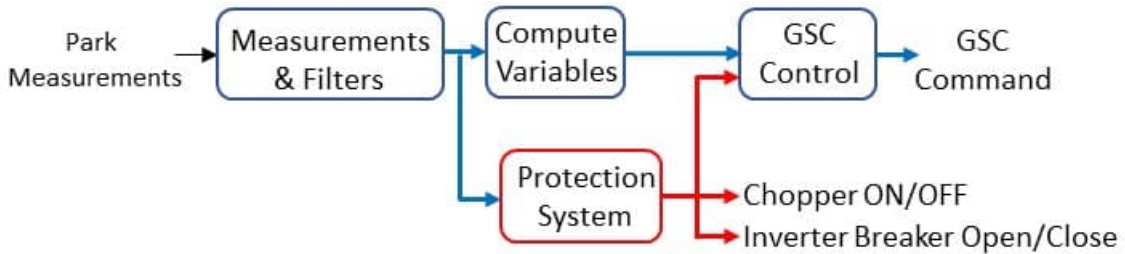


Figure 8 Simplified diagram of inverter control and protection system

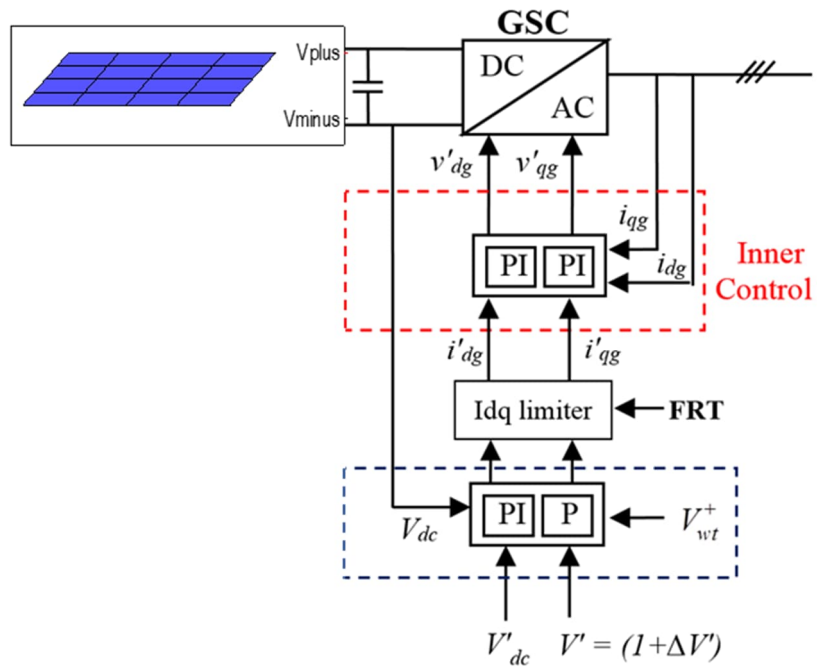


Figure 9 Schematic diagram of inverter control

3 EMTP® IMPLEMENTATION

The developed Solar panel model setup in EMTP is encapsulated using a subcircuit with a programmed mask as illustrated in Figure 10.

The first tab of the Solar panel mask enables the user to modify the general Solar panel parameters (**array rated power, voltage and frequency, filter characteristics and Dc voltage.**) and Solar panel operating conditions (**operating mode and reactive power at POI**).

The third tab is used to modify the parameters of converter control system given below:

- **Sampling rate and PWM frequency at PV converters**
- **PV inverter input measuring filter parameters,**
- **GSC control parameters,**

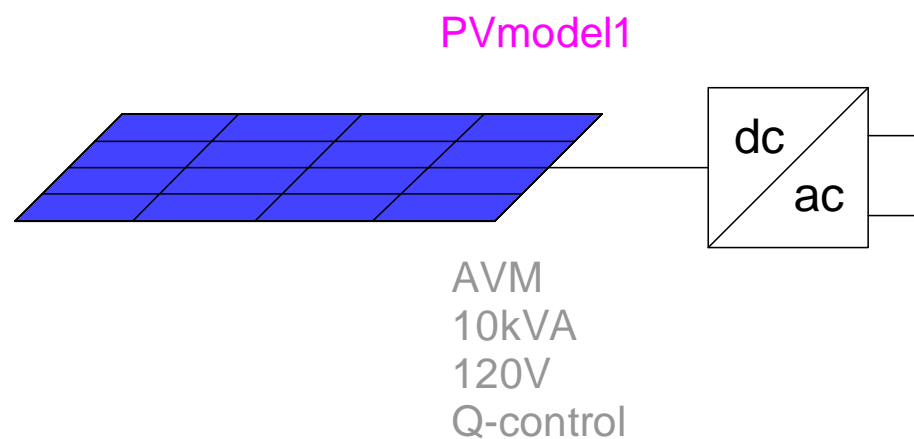


Figure 10 Solar panel device.

3.1 Detailed and Average Value Models

The EMTP® diagram of the PV dc-ac converter system detailed model (DM) is shown in Figure 11. A detailed two-level topology (Figure 12.a) is used for the VSCs in which the valve is composed by one IGBT switch, two non-ideal (series and anti-parallel) diodes and a snubber circuit as shown in Figure 12.b. The non-ideal diodes are modeled as non-linear resistances. The DC resistive chopper limits the DC bus voltage and is controlled by protection system block.

The PWM block in dc-ac converter system EMTP® diagram receives the reference voltage from converter control and generates the pulse pattern for the four IGBT switches by comparing the voltage reference with a triangular carrier wave. In a two-level converter, if the reference voltage is higher than the carrier wave then the phase terminal is connected to the positive DC terminal, and if it is lower, the phase terminal is connected to the negative DC terminal. The EMTP diagram of the PWM block is presented in Figure 13.

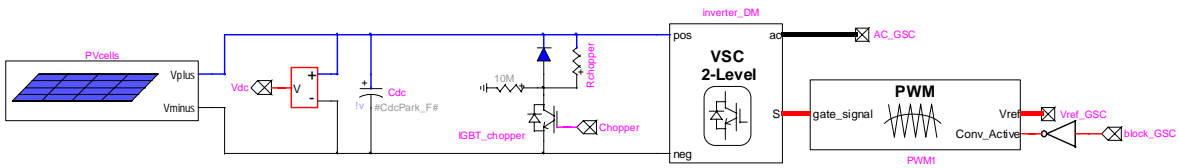


Figure 11 dc-ac converter system block in PV models (detailed model version)

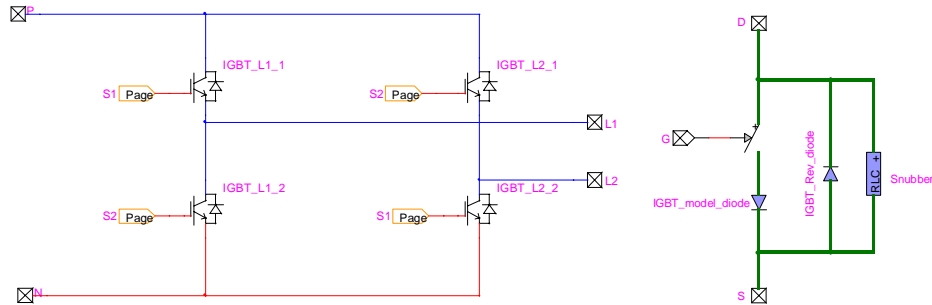


Figure 12 (a) Two-level Converter, (b) IGBT valve

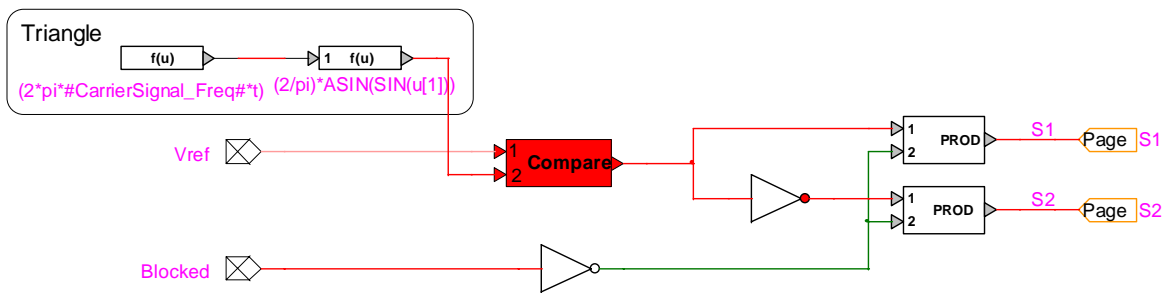


Figure 13 PWM control block

The DM mimics the converter behavior accurately. However, simulation of such switching circuits with variable topology requires many time consuming mathematical operations and the high frequency PWM signals force small simulation time step usage. These computational inefficiencies can be eliminated by using average value model (AVM) which replicates the average response of switching devices, converters and controls through simplified functions and controlled sources [11]. AVMs have been successfully developed for wind and solar generation technologies [12], [13]. AVM obtained by replacing DM of converters with voltage-controlled sources on the ac side and current-controlled sources on the dc side as shown in Figure 14.

The converter control tab of the Solar panel device mask enables used AVM-DM selection.

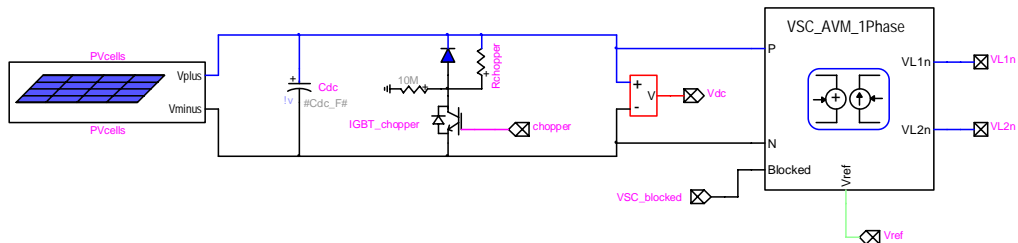


Figure 14 dc-ac converter system block in PV models (average value model version)

3.2 Solar panel Model in EMTP®

The EMTP® diagram of the Solar panel is shown in Figure 15. It is composed of

- “PV hardware” block which contains the PV panel and the inverter,
- “PV Control System” block,
- “Solar panel Control System” block,
- Initialization Source with load flow (LF) constraint.

The initialization source contains the load flow constraints. It also prevents large transients at external network during initialization of PV electrical and control systems.

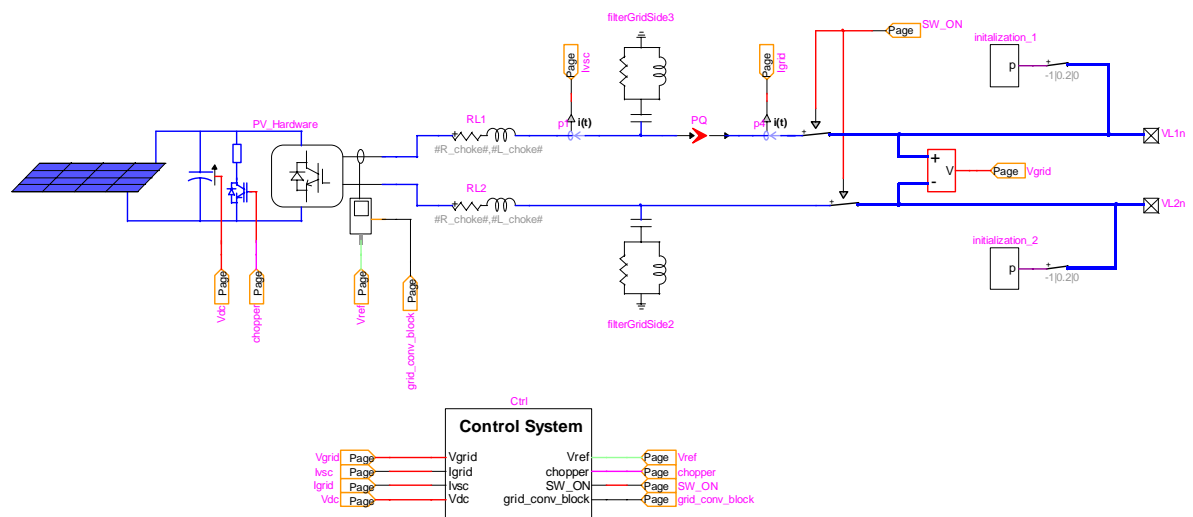


Figure 15 EMTP® diagram of the Solar panel

3.2.1 Solar panel Control System Block

The function adjusts the PV inverter controller voltage reference to achieve desired reactive power at POI. The reactive power control block consists in an outer voltage (or power factor) control and a slow inner proportional-integral reactive power control as shown in Figure 16. The reactive power reference for the inner proportional-integral reactive power control is produced either by the outer proportional voltage control (V-control) or by the outer power factor control (pf-control) unless Q-control is selected.

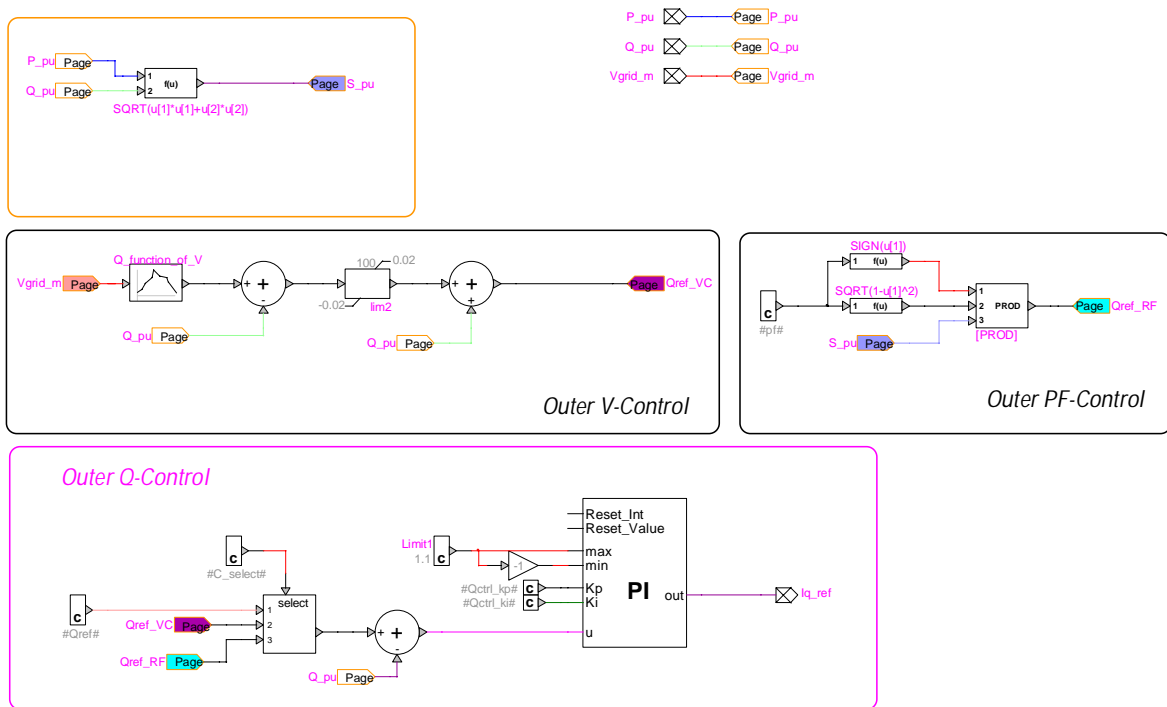


Figure 16 EMTP® diagram of the Q-control block

3.2.2 PV Electrical System

The EMTP® diagram of the electrical system is composed of the PV panel, the dc-ac converter system, the choke filter and the shunt ac harmonic filters as shown in Figure 17.

The measurement blocks are used for monitoring and control purposes. The monitored variables are GSC and total PV unit currents, and converter terminal voltages. The dc voltage is also monitored (in dc-ac converter system block). All variables are monitored as instantaneous values and meter locations and directions are shown in Figure 17.

The dc-ac converter system block details have been presented in Section 3.1.

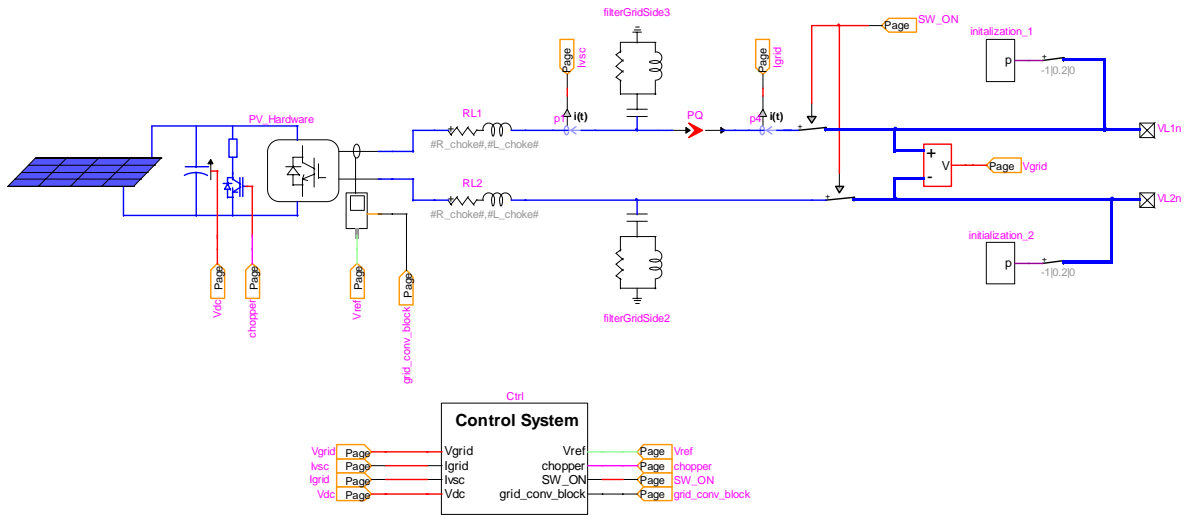


Figure 17 EMTP® diagram of the Solar panel

The “shunt ac harmonic filters” block includes two band-pass filters as shown in Figure 18. These filters are tuned at switching frequencies harmonics n_1 and n_2 . The filter parameters are computed as

$$C_{f1} = \frac{Q_{filter}}{U^2(2\pi f)} \quad (31)$$

$$L_{f1} = \frac{1}{C_{f1}(2\pi f n_1)^2} \quad (32)$$

$$R_{f1} = (2\pi f)n_1 L_{f1} Q \quad (33)$$

$$C_{f2} = C_{f1} \quad (34)$$

$$L_{f2} = \frac{1}{C_{f2}(2\pi f n_2)^2} \quad (35)$$

$$R_{f2} = (2\pi f)n_2 L_{f2} Q \quad (36)$$

where U is the rated LV grid voltage, Q_{filter} is the **reactive power of the filter** and Q is the **quality factor**.

The switching frequencies harmonics n_1 and n_2 are as follows

$$n_1 = f_{PWM-gsc} / f_s \quad (37)$$

$$n_2 = 2n_1 \quad (38)$$

where $f_{PWM-gsc}$ is the **PWM frequency** at GSC and f_s is the **nominal frequency**.

In case another type of filter or other parameters should be used, the filter can be modified by the user inside the Solar panel subcircuit. If several Solar panels are found in the network, the filter subcircuit and its parents must be made unique to avoid modifying all Solar panel instances.

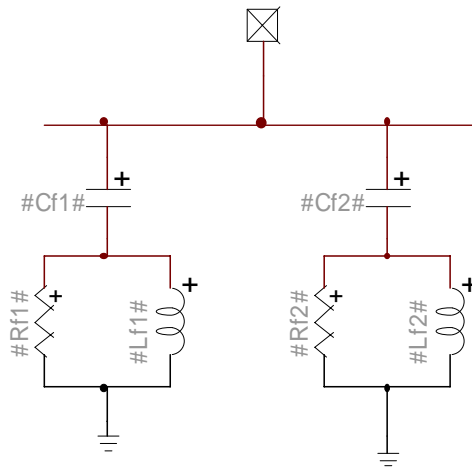


Figure 18 “shunt ac harmonic filter” block

3.2.3 PV inverter Control System Block

The EMTF[®] diagram of the PV inverter control system block is shown in Figure 19. The sampled signals are converted to pu and filtered. The sampling frequency are set to 12.5 kHz from device mask and can be modified by the user. The “sampling” blocks are deactivated in AVF due to large simulation time step usage. In generic model, 2nd order Bessel type low pass filters are used. The cut-off frequencies of the filters are set to 2.5 kHz and can be modified by the user. The order (up to 8th order), the type (Bessel and Butterworth) and the cut-off frequencies of the low pass filters can be modified from device mask. The “GSC Compute Variables” block does the dq transformation required for the vector control. The GSC (“Grid Control” block) operates in the stator voltage reference frame. The protection block includes the over/under voltage relay, the deep voltage sag detector, the dc chopper control and overcurrent detector.

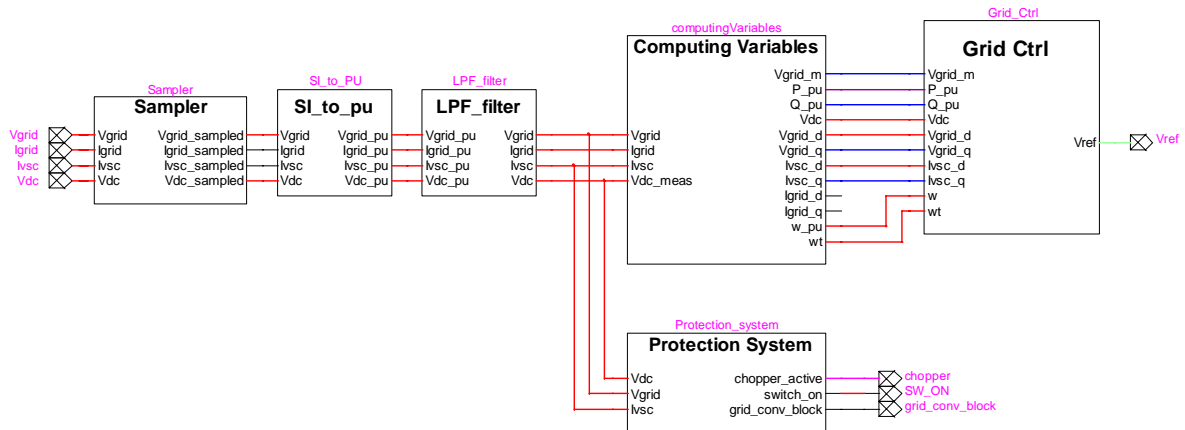


Figure 19 EMTF[®] diagram of the PV inverter control block

The transformation matrix T in (39) transforms the phase variables into two quadrature axis (d and q reference frame) components rotating at synchronous speed $\omega = d\theta / dt$. The phase angle θ of the rotating reference frame is derived by a PLL (see Figure 20) from the PV inverter terminal voltages allowing the synchronization of the control parameters with the system voltage. In matrix T , the direct axis d is aligned with the stator voltage.

$$T = \frac{2}{3} \begin{bmatrix} \cos(\omega t) & \cos(\omega t - 2\pi/3) & \cos(\omega t + 2\pi/3) \\ -\sin(\omega t) & -\sin(\omega t - 2\pi/3) & -\sin(\omega t + 2\pi/3) \\ 1/2 & 1/2 & 1/2 \end{bmatrix} \quad (39)$$

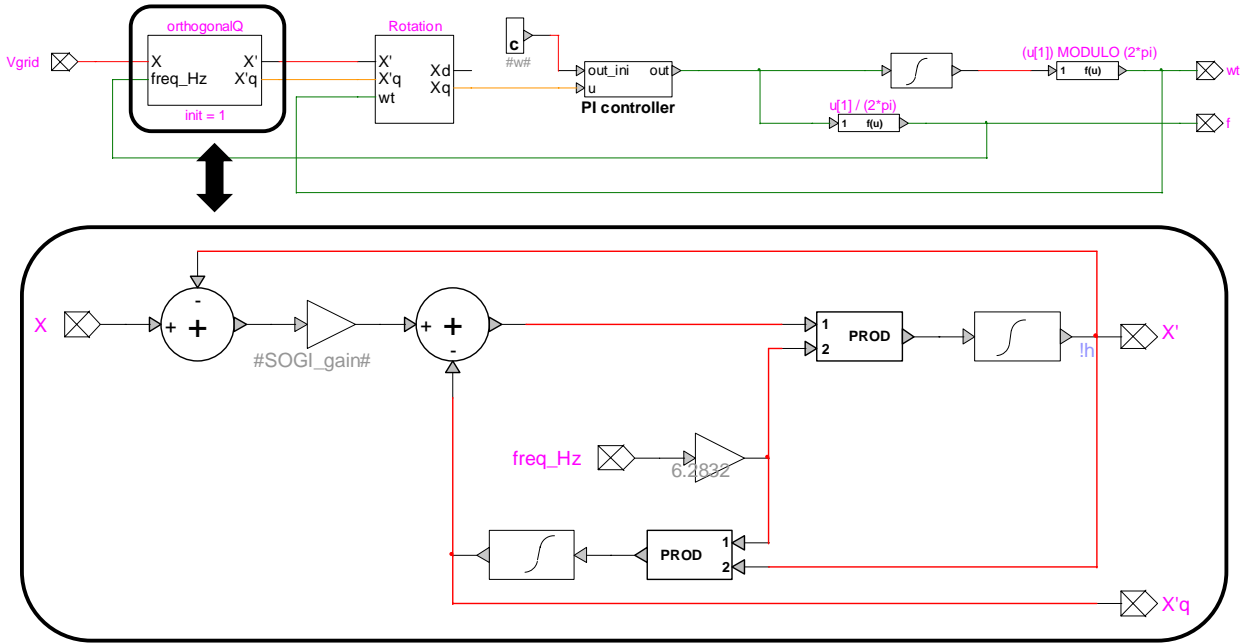


Figure 20 EMTP diagram of the PLL

3.2.3.1 PV inverter Grid Side Converter Control

The function of GSC is maintaining the dc bus voltage V_{dc} at its nominal value and controlling the reactive power on the grid side. The EMTP® diagram of the “Grid Control” block is shown in Figure 21.

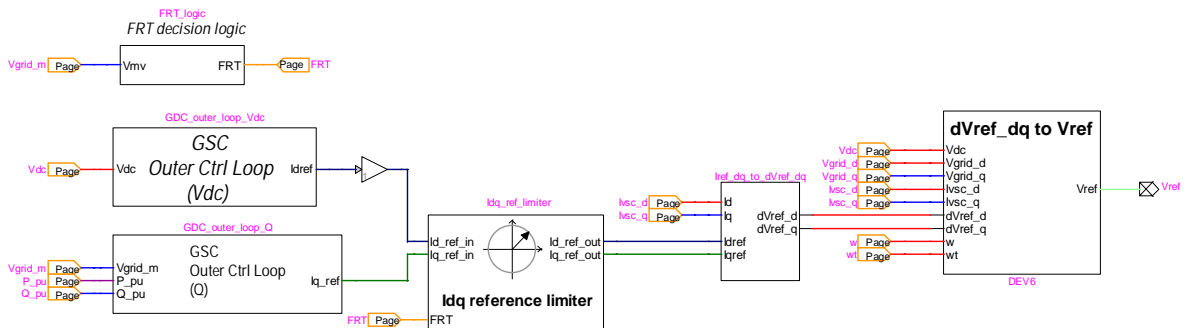


Figure 21 EMTP® diagram of PV inverter “Grid Control” block

3.2.3.1.1 PV inverter GSC Coupled Control

The q-axis reference current is calculated by the reactive power control block (see 2.1).

The d-axis reference current is calculated by the proportional outer dc voltage control. It is a PI controller tuned based on inertia emulation.

$$k_p = \omega_0^2 (2H_{Cdc}) \quad (40)$$

$$k_i = 2\xi\omega_0(2H_{Cdc}) \quad (41)$$

where ω_0 is the natural frequency of the closed loop system and ξ is the damping factor. $H_{Cdc} = (E_{Cdc}/S_{wt})$ is the static moment of inertia, E_{Cdc} is the stored energy in dc bus capacitor (in Joules) and S_{wt} is the Solar panel rated power (in VA).

The schematic of the GSC connected to the power system is shown in Figure 22. $Z = R + j\omega L$ represents the grid impedance including the transformers as well as the choke filter of the GSC. The voltage equation is given by

$$\mathbf{v}_{grid_i} = \mathbf{R} \mathbf{i}_{ac_i} - \mathbf{L} (d \mathbf{i}_{ac_i} / dt) + \mathbf{v}_{ac_i} \quad (42)$$

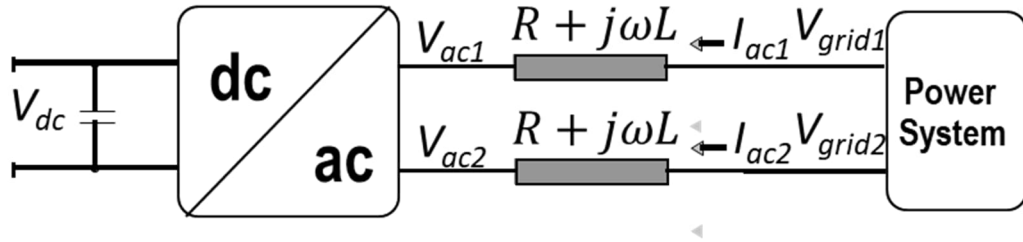


Figure 22 GSC arrangement

The link between GSC output current and voltage can be described by the transfer function

$$G_{gsc}(s) = 1/(R + sL) \quad (43)$$

Using [15], the PI controller parameters of the inner current control loop are found as

$$k_p = \alpha_c L \quad (44)$$

$$k_i = \alpha_c R \quad (45)$$

The feed-forward compensating terms $\omega L_{choke} i_{qg} + v_{d-choke}$ and $(-\omega L_{choke} i_{dg} + v_{q-choke})$ are added to the d- and q-axis voltages calculated by the PI regulators, respectively. The converter reference voltages are as follows

$$v'_{dg} = -(k_p + k_i/s)(i'_{dg} - i_{dg}) + \omega L_{choke} i_{qg} + v_{d-choke} \quad (46)$$

$$v'_{qg} = -(k_p + k_i/s)(i'_{qg} - i_{qg}) - \omega L_{choke} i_{dg} + v_{q-choke} \quad (47)$$

During normal operation, the controller gives the priority to the active currents, i.e.

$$\begin{aligned} i'_{dg} &< I_{dg}^{\lim} \\ i'_{qg} &< I_{qg}^{\lim} = \sqrt{(I_g^{\lim})^2 - (i'_{dg})^2} \end{aligned} \quad (48)$$

where I_{dg}^{\lim} , I_{qg}^{\lim} and I_g^{\lim} are the limits for d-axis, q-axis and total GSC currents, respectively.

The PV inverters are equipped with an FRT function to fulfill the grid code requirement regarding voltage support shown in Figure 23. The FRT function is activated when

$$\left|1 - V_{wt}^+\right| > V_{FRT-ON} \quad (49)$$

and deactivated when

$$\left|1 - V_{wt}^+\right| < V_{FRT-OFF} \quad (50)$$

after a pre-specified release time t_{FRT} .

When FRT function is active, the GSC controller gives the priority to the reactive current by reversing the d- and q-axis current limits given in (48), i.e.

$$\begin{aligned} i'_{qg} &< I_{qg}^{\text{lim}} \\ i'_{dg} &< I_{dg}^{\text{lim}} = \sqrt{\left(I_g^{\text{lim}}\right)^2 - \left(i'_{qg}\right)^2} \end{aligned} \quad (51)$$

The EMTP® diagram of “Idq reference limiter” and “FRT decision logic” blocks are given in Figure 24 and Figure 25, respectively. The limits for d-axis, q-axis and total GSC currents and FRT function thresholds can be modified from the device mask as shown in Figure 12.

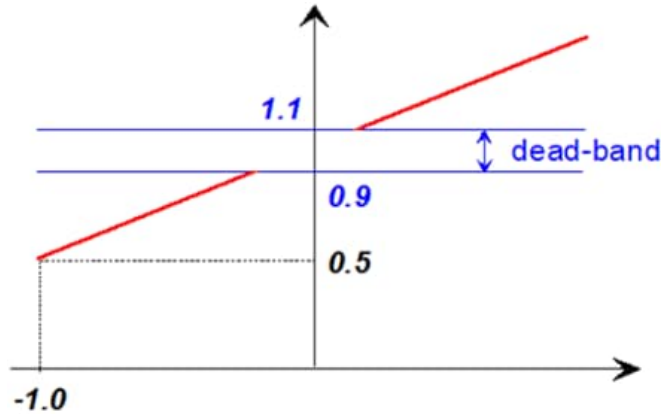


Figure 23 PV inverter reactive output current during voltage disturbances [16].

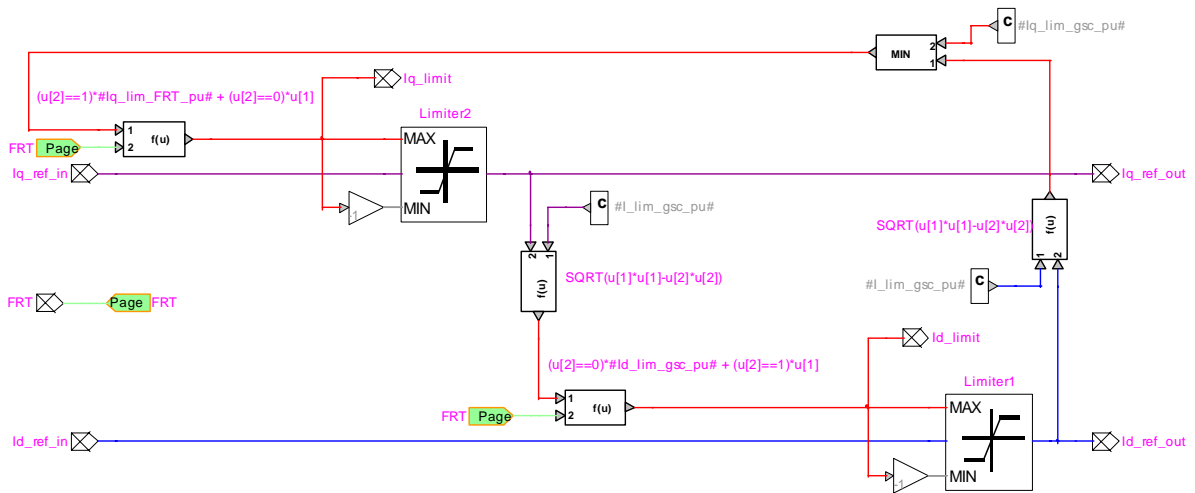


Figure 24 EMTP® diagram of “Idq reference limiter” block

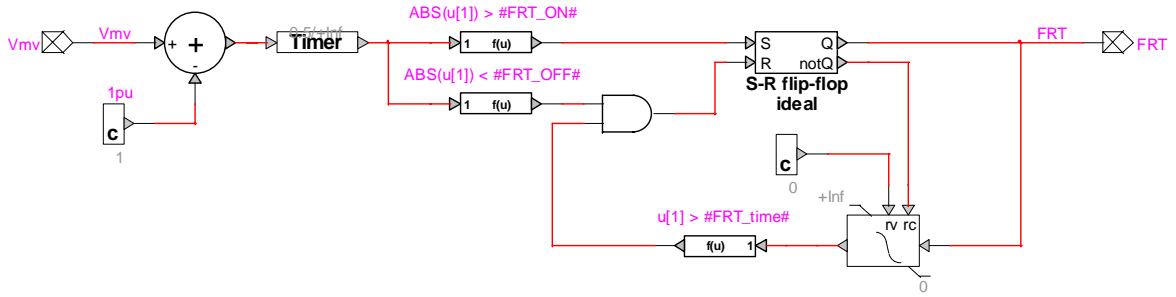


Figure 25 EMTP® diagram of “FRT decision logic” block

3.2.4 PV inverter Protection System Block

Figure 26 shows the “protection system” block. It includes overvoltage and undervoltage protection relays, a dc overvoltage protection (chopper protection) and an overcurrent detector for each converter to protect IGBT devices when the system is subjected to overcurrent. For initialization, all protection systems, except for DC chopper protection, are activated after 100ms of simulation (i.e. $init_Prot_delay = 0.1s$). The protection system parameters can be modified from the device mask as shown in Figure 27.

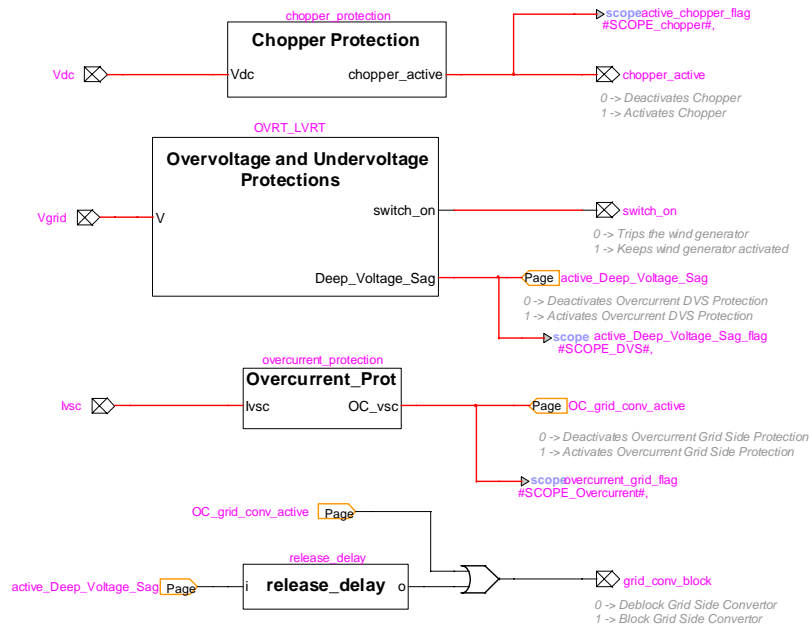


Figure 26 EMTP® diagram of protection system block

Voltage sag protection

Enable

Pickup DVS voltage pu

Reset DVS voltage pu

Chopper protection

Enable

Pickup V_{DC} pu

Reset V_{DC} pu

Overcurrent

Converter pickup current pu

Reset delay s

LVRT

Enable

	t (s)	V (pu)
1	0.15	0.01
2	0.175	0.03
3	0.255	0.1
4	0.5	0.14
5	0.625	0.16
6	0.7	0.25
7	1.0	0.75

[Preview characteristic plot](#)

OVRT

Enable

	t (s)	V (pu)
1	0.01	1.8
2	0.03	1.4
3	0.1	1.25
4	2.0	1.2
5	30	1.15
6	300	1.1
7		

[Preview characteristic plot](#)

Instantaneous Overvoltage Protection

Enable

	t (s)	V (pu)
1	0.000001	2
2	0.0016	1.7
3	0.003	1.4
4	0.016	1.3
5	1e5	1.299
6		
7		

[Preview characteristic plot](#)

Figure 27 Protection system parameters

3.2.4.1 Overvoltage and Undervoltage protections

Figure 28 shows overvoltage and undervoltage protections. It includes rms-based over/under voltage relays, cumulative instantaneous overvoltage relays, deep voltage sag detectors.

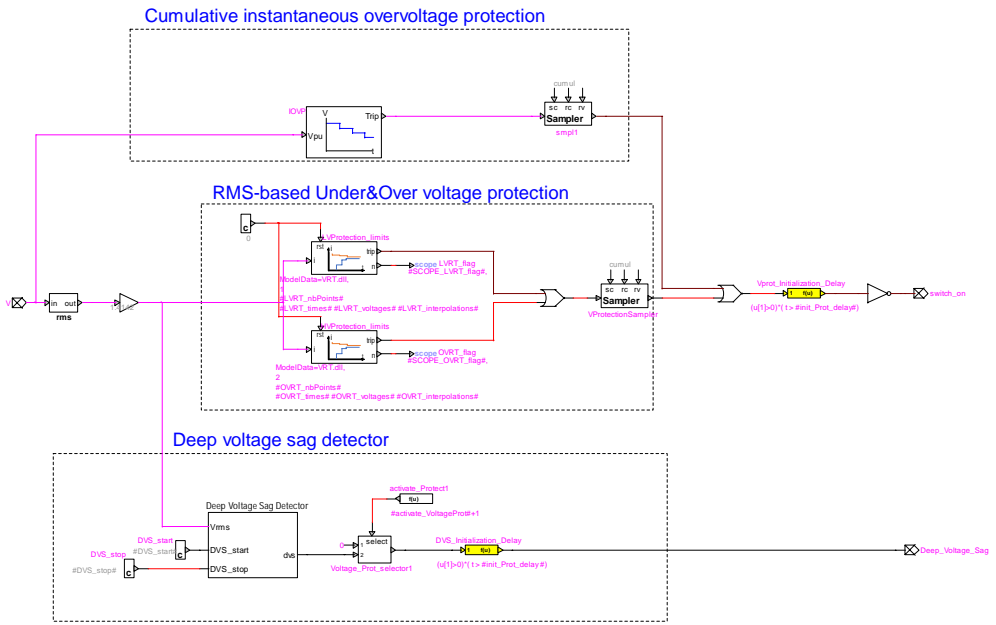


Figure 28 EMTP® diagram of overvoltage and undervoltage protections

The instantaneous over voltage protection suggested by IEEE Std 1547-2018 is developed and added to the protection schemes. This protection works based on a cumulative instantaneous overvoltage. Figure 29 shows the threshold values of the voltage (per unit of nominal instantaneous peak base) and cumulative duration of the transient overvoltage protection, and they can be modified in the device mask. The cumulative duration is the sum of durations when the instantaneous voltage exceeds the protection threshold over a one-minute time window.

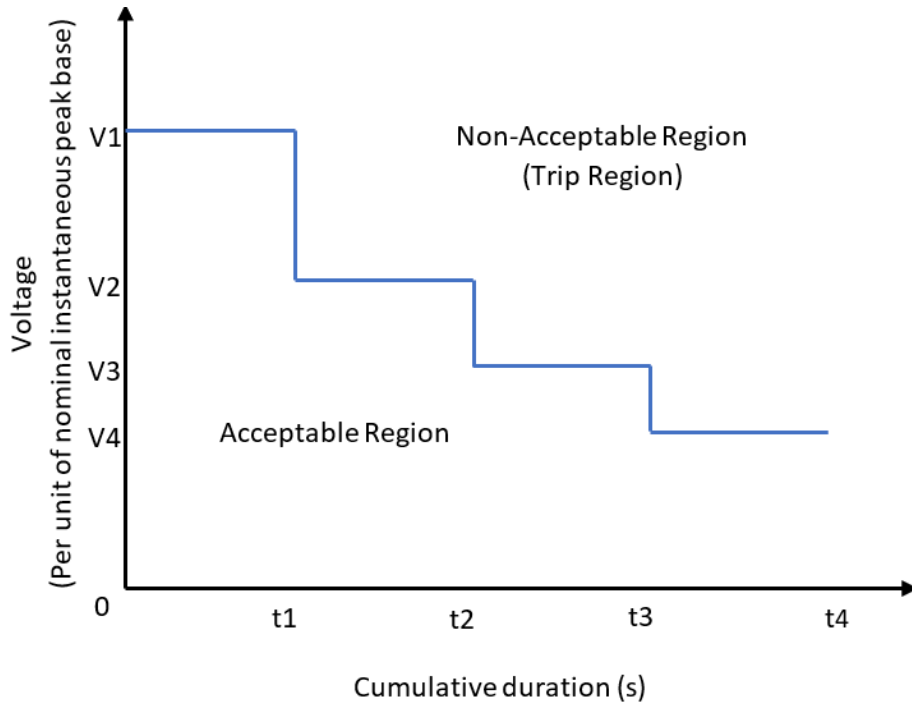


Figure 29 Transient overvoltage limits

The RMS-based over/under voltage protections are designed based on the technical requirements set by Hydro Quebec for the integration of renewable generation. The over/under voltage limits as a

function of time are presented in Figure 30 and can be modified in the PV device mask. The voltages below the red line reference and above the black line reference correspond to the ride-through region where the PV park is supposed to remain connected to the grid. This block measures the rms voltages on each phase and sends a trip signal to the PV inverter circuit breaker when any of the phase rms voltage violates the limits.

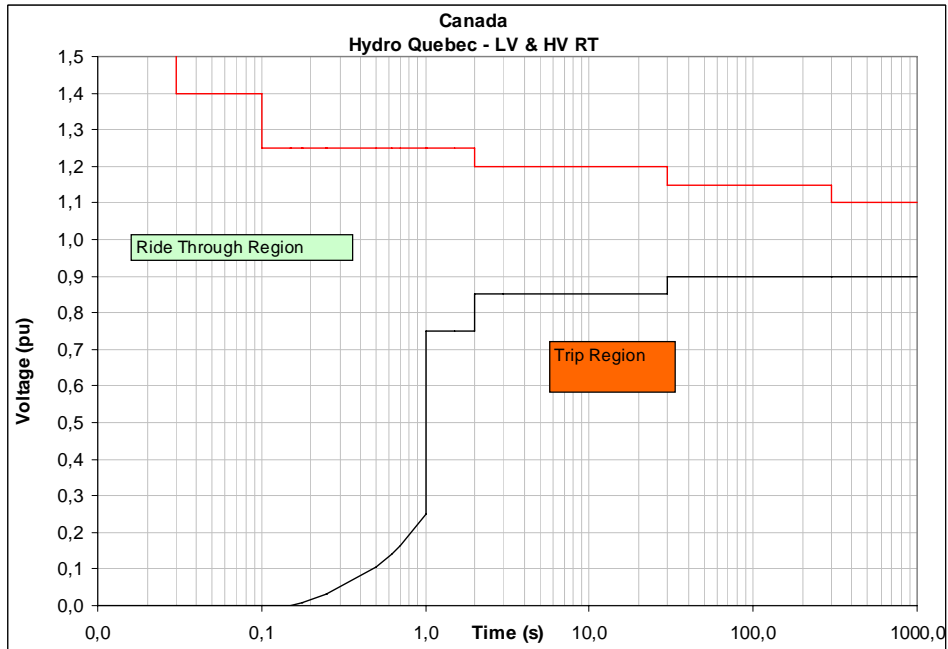


Figure 30 LVRT and HVRT requirements [19]

The “Deep Voltage Sag Detector” block temporarily blocks the GSC in order to prevent potential overcurrents and restrict the FRT operation to the faults that occur outside the PV park.

3.2.4.2 dc Overvoltage Protection Block

The function of dc chopper is to limit the dc bus voltage. It is activated when the dc bus voltage exceeds $|U_{chopper-ON}|$ and deactivated when dc bus reduces below $|U_{chopper-OFF}|$. EMTF diagram of the “dc overvoltage protection” is shown in Figure 31.

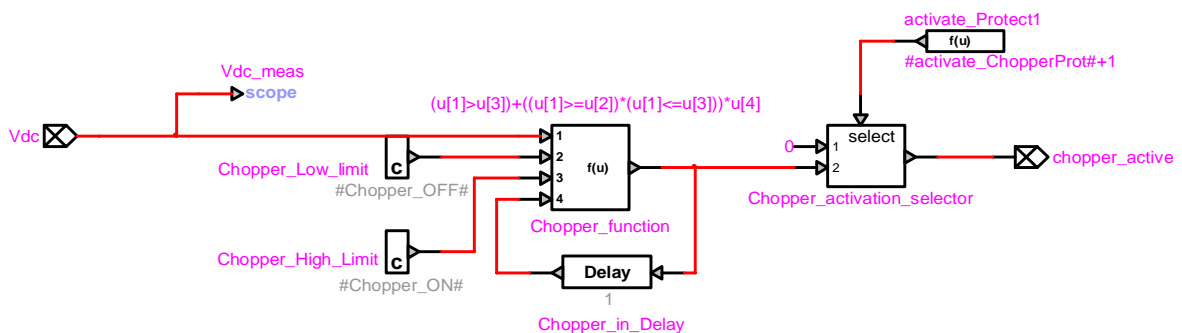


Figure 31 EMTF® diagram of dc overvoltage protection block

3.2.4.3 Overcurrent Protection Block

The overcurrent protection shown in Figure 32 blocks the converter temporarily when the converter current exceeds the pre-specified limit.

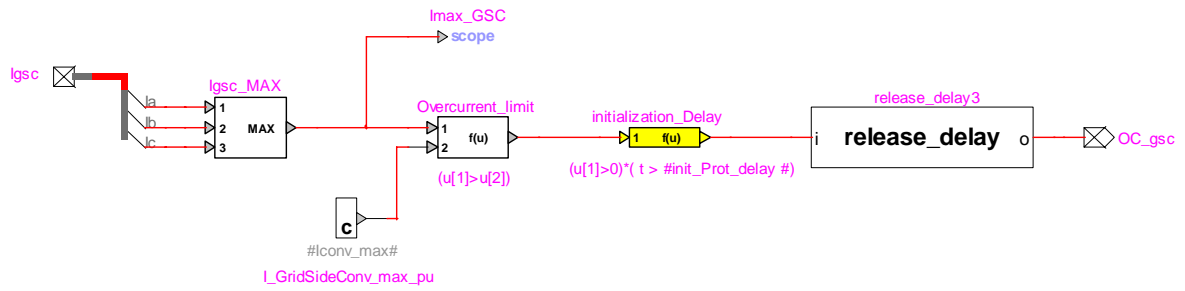


Figure 32 EMTP® diagram of overcurrent protection block

4 REFERENCES

- [1] Chih Hao Chang, Jia-Jun Zhu and Huan-Liang Tsai. "Modelbased performance diagnosis for PV systems", SICE, 2010, pp. 2139-2145.
- [2] G. H. Yordanov, O. M. Midtgård, T. O. Saetre, "PV Modules with Variable Ideality Factors", in 38th IEEE Photovoltaic Specialists Conference, 2012, p. 002362.
- [3] V. Sangsawang, S. Chaitusaney, "Modeling of Photovoltaic Module from Commercial Specification in Datasheet", in 9th ECTI Conference, Phetchaburi, Thailand, May 16-18, 2012, pp. 1-4.
- [4] U. Karaagac, J. Mahseredjian and L. Cai, "High Voltage Ride-Through Capability of DFIG-based Solar panels with FACTS," Proc. of 13th International Workshop on Large-Scale Integration of Wind Power into Power Systems, Berlin, Germany, Nov. 2014.
- [5] O. Anaya-Lara, N. Jenkins, J. Ekanayake, P. Cartwright, and M. Hughes, Wind Energy Generation: Modelling and control, Wiley, 2009, John Wiley & Sons, Ltd.
- [6] N. W. Miller, W. W. Price, and J. J. Sanchez-Gasca, "Dynamic modeling of GE 1.5 and 3.6 wind turbine-generators," GE-Power System Energy Consulting, General Electric International, Inc., Schenectady, NY, USA, Oct. 2003.
- [7] G. Abad, J. Lopez, M. A. Rodriguez, L. Marroyo, G. Iwanski, Doubly Fed Induction Machine: Modeling and Control for Wind Energy Generation, 2011, Wiley.
- [8] M. Singh, S. Santoso, Dynamic Models for Wind Turbines and Wind Power Plants, 2011.
- [9] J. M. Garcia, "Voltage control in wind power plants with doubly fed generators," Ph.D. thesis, Alaborg Univ., Denmark, Sep. 2010.
- [10] V. Akhmatov, A. H. Nielsen, J. K. Pedersen, O. Nymann, "Variable-speed wind turbines with multi-pole synchronous permanent magnet generators. Part I: Modelling in dynamic simulation tools", Wind Eng., vol. 27, no. 6, pp. 531-548, Dec. 2003.
- [11] S. R. Sanders, J. M. Noworolski, X. Z. Liu, and G. C. Verghese, "Generalized averaging method for power conversion circuits," IEEE Trans. on Power Electron, vol. 6, no. 2, pp. 251–259, Apr. 1991.
- [12] J. Morren, S. W. H. de Haan, P. Bauer, J. Pierik, and J. Bozelie, "Comparison of complete and reduced models of a wind turbine with Doubly-fed Induction Generator," in Proc. 10th Eur. Conf. Power Electron. Appl., Toulouse, France, Sep. 2003.
- [13] J. G. Slootweg, H. Polinder, and W. L. Kling, "Representing wind turbine electrical generating systems in fundamental frequency simulations," IEEE Trans. on Energy Conv., vol. 18, no. 4, pp. 516-524, Dec. 2003.
- [14] P. Rodriguez , J. Pou , J. Bergas , I. Candela , R. Burgos and D. Boroyevich, "Double synchronous reference frame PLL for power converters", Proc. IEEE PESC, pp. 1415-1421, 2005
- [15] L. Harnefors and H. Nee, "Model-based current control of ac machines using the internal model control", IEEE Trans on Ind. Appl., pp. 133-141, Jan/Feb. 1998.
- [16] "Grid code - high and extra high voltage," E.ON Netz GmbH, Bayreuth, Germany, April 2006.

- [17] R. Teodorescu, M. Liserre, P. Rodriguez, *Grid Converters for Photovoltaic and Wind Power Systems*, 2011, IEEE/Wiley.
- [18] Rodriguez, P., Pou, J., Bergas, J., Candela, J. I., Burgos, R.P. and Boroyevich, D., "Decoupled Double Synchronous Reference Frame PLL for Power Converters Control", *IEEE Transactions on Power Electronics*, 22, March 2007, 584–592.
- [19] *Transmission Provider Technical Requirements for the Connection of Power Plants to the Hydro-Quebec Transmission System*, Hydro Quebec Transenergie, 2009.
- [20] G. R. Slemon, "Modelling of induction machines for electric drives," *IEEE Transactions on Industry Applications*, 25(6):1126-31, 1989.
- [21] R. Pena, J. C. Clare, G.M. Asher, "Doubly fed induction generator using back to back PWM converters and its application to variable-speed wind-energy generation", *IEE Proc. Electr. Power Appl.*, No.3. pp.231-240, 1996.
- [22] Muljadi, T. Batan, D. Yildirim, C. Butterfield, "Understanding the unbalanced voltage problem in wind turbine generation *Proc. Ind. Appl. Conf.*, pp. 1359–1365.
- [23] T.K.A. Brekken, N. Mohan, "Control of a doubly fed induction wind generator under unbalanced grid voltage conditions," *IEEE Trans. Energy Convers.*, Vol: 22, No: 1, pp. 129-135, March 2007.
- [24] L. Xu, Y. Wang, "Dynamic modeling and control of DFIG-based wind turbines under unbalanced network conditions," *IEEE Trans. Power Syst.*, Vol: 22, No: 1, pp. 314-323, Feb. 2007.
- [25] R. Pena, R. Cardenas, E. Escobar, "Control system for unbalanced operation of stand-alone doubly fed induction generators," *IEEE Trans. Energy Convers.*, Vol: 22, No: 2, pp. 544–545, June 2007.
- [26] H. Yin, L. Fan, R. Kavasseri, "Negative sequence compensation techniques of dfig-based wind energy systems under unbalanced grid conditions," *Proc. IEEE Power Electronics and Machines in Wind Applications (PEMWA)*, Lincoln, NE, 2009.
- [27] L. Fan, H. Yin, Z. Miao, "A novel control scheme for DFIG-based wind energy systems under unbalanced grid conditions," *Electric Power Systems Research*, Vol: 81, No:2, pp. 254–262, Feb. 2011.
- [28] T. Kauffmann, U. Karaagac, I. Kocar, H. Gras, J. Mahseredjian, B. Cetindag and E. Farantatos, "Phasor Domain Modeling of Type III Wind Turbine Generator for Protection Studies," *Proc. of IEEE PES General Meeting*, Denver, CO, USA, July 2015
- [29] U. Karaagac, T. Kauffmann, I. Kocar, H. Gras, J. Mahseredjian, B. Cetindag and E. Farantatos, "Phasor Domain Modeling of Type-IV Wind Turbine Generator for Protection Studies," *Proc. of IEEE PES General Meeting*, Denver, CO, USA, July 2015.
- [30] T. Kauffmann; U. Karaagac; I. Kocar; S. Jensen; J. Mahseredjian; E. Farantatos, "An Accurate Type III Wind Turbine Generator Short Circuit Model for Protection Applications," in *IEEE Trans. on Power Delivery*, doi: 10.1109/TPWRD.2016.2614620.
- [31] E. Muljadi, C.P. Butterfield, a Ellis, J. Mechenbier, J. Hochheimer, R. Young, N. Miller, R. Delmerico, R. Zavadil and J.C. Smith, "Equivalencing the collector system of a large wind power plant", 2006 IEEE PES General Meeting.

- [32] U. Karaagac, J. Mahseredjian, L. Cai, "Ferroresonance conditions in Solar panels", Electric Power Systems Research, Vo: 138, pp 41-49, Sep. 2016.